Kuwait J. Sci. **46 (3)** pp. 71-82, 2019

A flat-joint contact model and meso-analysis on mechanical characteristics of brittle rock

Yu Zhou[1], Nengbin Chen[1,*], Li Wang[2], Jianwang Li[3], Tianhua Wu[1]

[1]*Key Laboratory of Ministry of Education for Efficient Mining and Safety of Metal Mine, University of Science and Technology Beijing 100083, China*

[2]*PowerChina Road Bridge Group Co., Ltd., 100048 Beijing, China*

[3]*China Railway 16th Bureau Group Co., Ltd., Beijing 100018, China*

Corresponding author: 18692939718@163.com

Abstract

At present, it is difficult to simulate the mechanical characteristics of brittle rock, such as particle structure and the ratio of uniaxial tensile to uniaxial compressive strength (σ_t/σ_{ucs}), in the traditional particle model. Based upon particle flow theory and particle flow code (PFC), the flat-joint contact model is used to construct the granite meso-analysis model, which can reflect the mineral structure features. The failure modes of rock under uniaxial tension, uniaxial compression and tri-axial compression are simulated and compared with the experimental results. The results show that the model has a good performance in the study of brittle rock mechanics and the mechanical mechanism of brittle rock during failure process is deeply revealed from meso-mechanical viewpoint. Research also shows that for hard brittle rock such as granite, the lower ratio of uniaxial tensile to uniaxial compressive strength of the rock can be reproduced using the flat-joint contact model to construct a calculation model. Its strength characteristics can be more reasonably described using the Hoek-Brown strength criterion.

Keywords: Brittle; flat-joint contact model; fracture; granite; meso-analysis; strength

1. Introduction

As a typical brittle rock, granite often forms well-developed and visually discernible mineral particles, and is widely distributed in the upper continental crust. The macroscopic mechanical behavior of granite often depends on its micro- or meso-structure. therefore, to carry out the microscopic study of the mechanical behavior of granite is an important guarantee for rational design and safe construction of the project.

Granite microstructure type can be divided into an irregular polygon of the full crystal structure, semi-self-shaped structure and semi-crystalline structure, it reflects the environment of magma in the shallow crust, slowly cooling the crystallization and the normal precipitation sequence of minerals. In terms of mineral particle diameters, granite can be divided into coarse particles, medium particles and fine particles. On a microscopic scale, the granite specimen structure has an irregular polygonal crystal structure.

On the basis of the discrete element method, Cundall & Strack (1979) introduced the idea of molecular dynamics and created a particle flow method and PFC program. These are mainly used in the study of rock and concrete mechanics and engineering. The mechanism of damage and fracture of material is explained from the point of view of micromechanics, while the process of deformation and fracture is analyzed from linear elasticity to fracture. At present, many scholars have adopted the granular flow method and PFC program to carry out microscopic study of the mechanical behavior of granite. Hazzard & Young (2000) built a simulation method for the emission activity of granite on the mesoscale. Su & Li (2011) studied the spatial and temporal distributions of acoustic emission (AE) during the deformation of granite samples containing an inhomogeneous fault under confinement using the PFC program. According to the physical and mechanical parameters from laboratory experiments and grains section scanning, Miao *et al.* (2013) built a micro-geometric model of migmatitic granite grains based on

particle flow theory and the PFC program. Loading codes were developed and some functions were adjusted by Fish language to simulate uniaxial and triaxial (σ_3= 40MPa) compression experiments. Zhou et al. (2018) used the PFC program to investigate the effect mechanism of fractures on the mechanics characteristics of jointed rock mass under compression. Li et al. (2019) investigated the effect of the interaction between cavities and flaws on rock mechanical properties under uniaxial compression using techniques combining of acoustic emission, computerized tomography (CT) and PFC program. However, these studies are based on the traditional particle model, namely, using disk or spherical particles to build the calculation model.

For hard and brittle rocks, Hoek & Brown (1997) found that the ratio of uniaxial tensile to uniaxial compressive strength is usually 0.04 to 0.03, i.e. σ_t/σ_{ucs} = 1/24 to 1/30. For the traditional particle model, Diederichs (2000) found that the meso-mechanical parameters of the particle model obtained by inversion of the uniaxial compression test result in high calculative uniaxial tensile strength, while at the same time causing calculative strength envelope linearly. This can only be described by the Mohr-coulomb strength criterion. Therefore, it results that the calculative and actual strength characteristics of a brittle rock sample vary greatly. In addition, Cho *et al.* (2007) also pointed out that the σ_t/σ_{ucs} calculated by the traditional particle model is usually about 0.25. Potyondy & Cundall (2004) analyzed the traditional particle model constructed by the disc or spherical particle unit. They found that it is not able to reflect the irregular structure of mineral particles in rock, which results in a lack of a self-locking effect between particles.

Wu & Xu (2016) studied the advantages of a flat-joint model for stimulating behavior of marble. Kazerani & Zhao (2010) analyzed the mechanics of brittle rock by using bonded particle modelling. Zhou *et al.* (2013) researched the Brazilian splitting test of hard brittle marble. Ding & Zhang (2014) analyzed the tensile strength of rock based on a new contact model. Zhou *et al.* (2016) used the discrete element method to study the behavior of crushable granular assemblies under true triaxial stress conditions. Go *et al.* (2014) proposed a new model to estimate the thermal conductivity of granite soils in Korea. Tang *et al.* (2014) presented a numerical simulation on rock failure process based on the characterization of rock heterogeneity.

Kazerani & Zhao (2010) analyzed the mechanics of brittle rock by using bonded particle modelling. Zhou *et al.* (2013) researched the Brazilian splitting test of hard brittle marble. Ding & Zhang (2014) analyzed the tensile strength of rock based on a new contact model. Go *et al.* (2014) proposed a new model to estimate the thermal conductivity of granite soils in Korea. Tang *et al.* (2014) presented a numerical simulation on rock failure process based on the characterization of rock heterogeneity. Wu & Xu (2016) studied the advantages of a flat-joint model for stimulating behavior of marble. Zhou *et al.* (2016) used the discrete element method to study the behavior of crushable granular assemblies under true triaxial stress conditions. However, these simulations on the mechanical properties of brittle rocks are difficult to meet the requirements of computational efficiency and accuracy.

In order to solve the shortcomings of the traditional particle model for simulating the mechanical properties of brittle rock, a new particle contact model, i.e. the flat-joint contact model, was used to construct the mesoscopic analysis model of granite. This model can reflect the irregular polygon structure of mineral particles. By comparing the calculated results with those of laboratory tests, the suitability and reliability of the flat-joint model in the study of rock mechanics were verified. At the same time, the fracture mechanism and strength characteristics of granite under the condition of uniaxial tension, uniaxial compression and triaxial compression were revealed from a meso-mechanical viewpoint.

2. Flat-joint contact model

The flat-joint contact model (FJM) is used to simulate the mechanical properties of an interface between two spheroidal particles. The interface consists of two flat notional surfaces (notional surfaces1, notional surfaces 2) which coincides with the interface in the center of contact plane of particles (see Figure 1). The interface is defined by the original point ($\hat{\mathbf{x}}_c$) and the unit normal and the shear vector ($\hat{\mathbf{n}}_c$, $\hat{\mathbf{t}}_c$). $\hat{\mathbf{x}}_c$ is the center of contact plane of particles, the direction of the vector $\hat{\mathbf{n}}_c$ is from the center of particle 1 pointing to the center of particle 2. The mechanical properties of the interface can be divided into bond and friction type and can vary along with the interface. If the mechanical property of interface is bonded, its mechanical state can evolve from a fully bonded state to a partly bonded state. It can then further evolve to a fully unbonded and frictional state. Since the parallel bond contact model of the particle peripheral contact has a certain length, particle assembly can behave as irregular polygons, which can reproduce the crystal structure of mineral particles of rock, as shown in Figure

5. During the calculation, the position and the mechanical state of the FJM can be determined by the kinematics equation and kinetic equation, respectively.

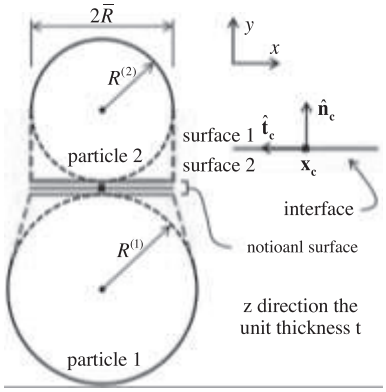

Fig. 1. Flat-joint contact model

2.1 Kinematics equation

The relative motion of the notional surfaces at the particle contact location is expressed by the relative translational velocity $\dot{\mathbf{U}}$ and the relative rotational velocity $\dot{\theta}$:

$$\begin{cases} \dot{\mathbf{U}} = \left[\dot{\mathbf{x}}_{\mathbf{c}}^{(2)} + \boldsymbol{\omega}^{(2)} \times \left(\mathbf{x}_{\mathbf{c}} - \mathbf{x}^{(2)}\right)\right] \\ \quad -\left[\dot{\mathbf{x}}_{\mathbf{c}}^{(1)} + \boldsymbol{\omega}^{(1)} \times \left(\mathbf{x}_{\mathbf{c}} - \mathbf{x}^{(1)}\right)\right], \\ \dot{\theta} = \boldsymbol{\omega}^{(2)} - \boldsymbol{\omega}^{(1)} \end{cases} \tag{1}$$

where $\dot{\mathbf{x}}$ is the center position of particle, $\dot{\mathbf{x}}$ and $\boldsymbol{\omega}$ are the translational and rotational velocity, respectively. The superscript is the number of the particle. $\dot{\mathbf{x}}_{\mathbf{c}}^{(\mathrm{i})}$ and $\dot{\mathbf{x}}^{(\mathrm{i})}$ are translational velocity and the central position of particle *i* at the particle contact location, respectively.

Relative translational and rotational velocity $\dot{\mathbf{U}}$ and $\dot{\theta}$ can also be denoted by:

$$\begin{cases} \dot{\mathbf{U}} = \dot{U}_n \hat{\mathbf{n}}_{\mathbf{c}} + \dot{U}_s \hat{\mathbf{t}}_{\mathbf{c}} \\ \dot{\theta} = \boldsymbol{\omega}^{(2)} - \boldsymbol{\omega}^{(1)} = \dot{\theta}\hat{\mathbf{k}} \end{cases}, \tag{2}$$

where $\dot{\mathbf{U}}_n$ and $\dot{\mathbf{U}}_s$ are the normal and tangential relative translational velocity of the notional surfaces, respectively; $\dot{\theta}$ is relative rotational velocity, $\hat{\mathbf{n}}_{\mathbf{c}}$ and $\hat{\mathbf{t}}_{\mathbf{c}}$ are unit vector of the X, Y-axis, respectively. Thus the relative displacement and rotation increments $\Delta\mathbf{U}$ and $\Delta\theta$ of every timestep $\Delta\mathbf{t}$ are given by:

$$\begin{cases} \Delta\mathbf{U} = \Delta U_n \hat{\mathbf{n}}_{\mathbf{c}} + \Delta U_s \hat{\mathbf{t}}_{\mathbf{c}} \\ \Delta\boldsymbol{\theta} = (\dot{\theta}\Delta t)\hat{\mathbf{k}} = \Delta\theta\hat{\mathbf{k}} \end{cases}. \tag{3}$$

The generalized relative displacement will be set at null (zero) when the FJM is applied at the contact location of the particle (initialize two coincident notional surfaces):

$$U_n = U_s = \theta = 0 \quad . \tag{4}$$

The total relative motion of the interface, that translation amount in the normal direction U_{n}, the translation amount in the shear direction U_{s} and the rotation amount θ of the interface, can be calculated by the following equation:

$$\begin{cases} U_n := U_n + \Delta U_n \\ U_s := U_s + \Delta U_s \\ \theta := \theta + \Delta\theta \end{cases}. \tag{5}$$

The relative motion of the interface will generate a gap amount between particles (Figure 2). The interface gap g (g>0 is open) is determined by Equation (6), where $\bar{\mathsf{R}}$ is the mean diameter of the contacted particles. Note that the gap is not affected by the relative shear movement.

$$g(\xi) = U_n + \theta(\xi - \bar{R}), \quad \xi \in [0, 2\bar{R}] \tag{6}$$

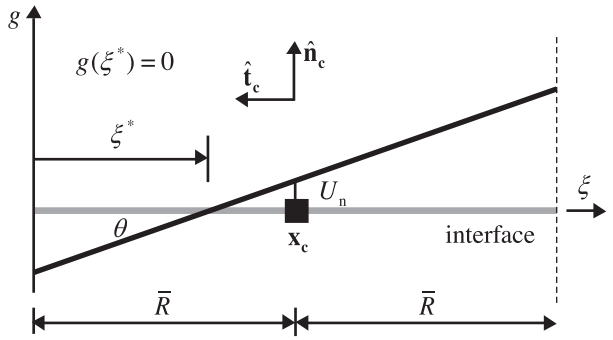

Fig. 2. Interface gap value

2.2 Kinetic equation

In the process of the relative motion of the notional surfaces, the force $\mathbf{F}_{\mathbf{c}}$ and moment $\mathbf{M}_{\mathbf{c}}$ at each contact are updated by the generalized force–displacement law. These forces and moments act at the twinning notional surface centroid in an equal and opposite sense. The interface is normally discretized into N segments of a segment of the same size. Each segment carries a force and moment ($\mathbf{F}^{(\mathrm{i})}$ and $\mathbf{M}^{(\mathrm{i})}$) that act at the element centroid in an equal and opposite sense on the notional surfaces (Figure 3).

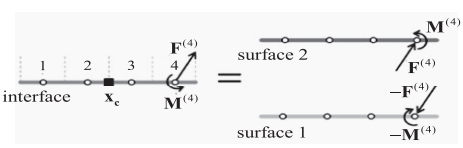

Fig. 3. Force and moment acting on segment center

The force $\mathbf{F_c}$ and moment $\mathbf{M_c}$ at the contact location can be calculated via the force and moment in these segments:

$$\begin{cases} \mathbf{F_c} = \sum_{i=1}^{N} \mathbf{F}^{(i)} \\ \mathbf{M_c} = \sum_{i=1}^{N} \left[\left(\mathbf{r}^{(i)} \times \mathbf{F}^{(i)} \right) + \mathbf{M}^{(i)} \right] \end{cases}, \tag{7}$$

where $\mathbf{r}^{(i)} = \mathbf{x}^{(i)} - \mathbf{x_c}$ is position vector, $\mathbf{x}^{(i)}$ is the center of segment i. In addition, vector $\mathbf{r}^{(i)}$ can be described as:

$$\mathbf{r}^{(i)} = \mathbf{x}^{(i)} - \mathbf{x_c} = \rho^{(i)} \hat{\mathbf{t}}_c \quad , \tag{8}$$

where $i = 1,2,\cdots,N$, $\rho^{(i)} = \bar{R}(\frac{-2i+1+N}{N})$.

Thus, a moment in the contact location can be described by Equation (9):

$$\begin{aligned} \mathbf{M_c} &= \sum_{i=1}^{N} \left\{ \rho^{(i)} \hat{\mathbf{t}} \times \left[F_n^{(i)} \hat{\mathbf{n}} + F_s^{(i)} \hat{\mathbf{t}}_c \right] + \mathbf{M}^{(i)} \right\} \\ &= \sum_{i=1}^{N} \left\{ -\rho^{(i)} F_n^{(i)} \hat{\mathbf{k}} + \mathbf{M}^{(i)} \right\} \end{aligned} \quad , \tag{9}$$

where the force on the segment can be decomposed into normal and tangential components ($\mathsf{F_n}$ and $\mathsf{F_s}$, $\mathsf{F_n} > 0$ means compression).

Each segment of interface obeys the force–displacement law. The force and moment of segment are updated according to the relative motion of the notional surfaces. Applying the law to each segment, the force and moment of contact can be acquired though Equation (8). the force-displacement response of the flat-joint interface is a self-adapting behavior that includes evolving from a fully bonded state to a fully unbonded and frictional state. The segment of interface obeys the force-displacement law described below.

Each element is either bonded ($\mathsf{B}^{(i)} \neq 0$) or unbonded ($\mathsf{B}^{(i)} = 0$). (See Figure 4.) Normal stress σ ($\sigma > 0$ means tension) of the interface can be described as:

$$\sigma(\xi) = L(\xi) k_n g \ , \xi \in [0, 2\bar{R}] \quad , \tag{10}$$

where $\mathsf{k_n}$ is normal stiffness of the flat-joint contact, $\mathsf{L}(\xi)$ is evaluated by:

$$\mathsf{L}(\xi) = \begin{cases} 1, \text{bonded} \\ 1, \text{unbonded}, \ \mathsf{g} < 0. \\ 0, \text{other} \end{cases} \tag{11}$$

Only a bonded segment can resist normal tensile stress, and all the segments share the same rectangular section area, which has size $\mathsf{A}^{(i)}$:

$$\mathsf{A}^{(i)} = \frac{2\bar{\mathsf{R}}\mathsf{t}}{\mathsf{N}} \quad , \tag{12}$$

where $\mathsf{t} = 1$, $\bar{\mathsf{R}} = \lambda \min\left(\mathsf{R}^{(1)}, \mathsf{R}^{(2)}\right)$.

The center of the segment carries normal and shear stress which are $\hat{\sigma}^{(i)} = -F_n^{(i)} / A^{(i)} (\hat{\sigma} > 0$, means tension) and $\hat{\tau}^{(i)} = F_s^{(i)} / A^{(i)}$. The normal and shear stress and moment of all segments will be set null (zero) when the FJM is applied at the contact location of a particle.

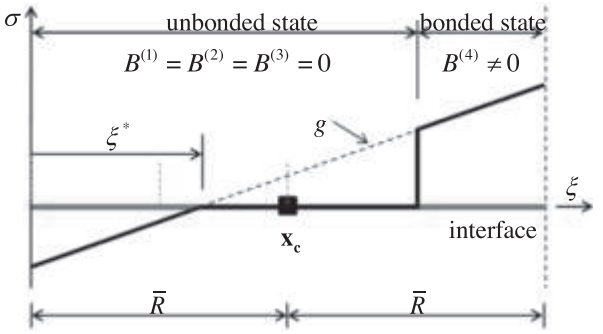

Fig. 4. Interface normal stress

In the process of the calculation, the force ($\mathsf{F_n}^{(i)}$, $\mathsf{F_s}^{(i)}$) and moment $\mathbf{M_c}$ of the segment are constantly updated by the generalized force–displacement law, and bond state ($\mathsf{B}^{(i)}$) is amended at the same time. $\mathsf{F_n}^{(i)}$ and $\mathsf{M}^{(i)}$ can be calculated by integrating the normal stress acting on the segment, while $\mathsf{F_s}^{(i)}$ can be acquired by calculating the increment. Its computational process can be formulated using the following three steps:

1) At the end of each timestep, calculate $\hat{\sigma}^{(i)}$ and bonded state based on the gap amount. If $B^{(i)} \neq 0$, $\hat{\sigma}^{(i)} > \sigma_b$, the bond is broken in tension via setting $B^{(i)} := \hat{\sigma}^{(i)} := \hat{\tau}^{(i)} := 0$, then skep to step 3) directly.

2) Calculate shear stress:

$$\hat{\tau}^{(i)'} := \hat{\tau}^{(i)} - k_s \Delta U_{se} \quad , \tag{13}$$

where $\mathsf{k_s}$ is flat-joint shear stiffness and $\Delta\mathsf{U_{se}}$ is elastic component of relative shear displacement increment. $\Delta\mathsf{U_{se}}$ is determined by the gap value at the segment centroid: if the segment is bonded, the whole increment is elastic; if the segment is unbonded, then the negative part of the gap value is elastic. The superscript *i* is removed in this process which is different from the description based on the bonded state.

For the unbonded segment, the shear strength is calculated as:

$$\tau_c = \begin{cases} -\mu\hat{\sigma}, \hat{\sigma} < 0 \\ 0, \hat{\sigma} \geq 0 \end{cases} \quad , \tag{14}$$

where μ is the friction coefficient. If $|\hat{\tau}'| \leq \tau_c$, then $\hat{\tau} := \hat{\tau}'$, otherwise the interface changes to a slip state via

setting $\hat{\tau} := \hat{\tau}'\left(\tau_c / \left|\hat{\tau}'\right|\right)$.

For the bonded segment, the shear strength is:

$$\tau_c = c_b - \bar{\sigma} \tan \phi_b \quad , \tag{15}$$

where c_b is cohesion, ϕ_b is friction angle. If $\left|\hat{\tau}'\right| \le \tau_c$, then $\hat{\tau} := \hat{\tau}'$, otherwise the bond is broken in shear via setting $B := \bar{\sigma} := \hat{\tau} := 0$.

Calculate the moment $M^{(i)}$ via the gap value and bonded state at the end of each timestep.

3. Experiment and calculation result analysis

3.1 Computational modeling

In this paper, mechanical tests of brittle rocks under different stress states were carried out by using medium-fine granodiorite from the 450 ~ 550m depth of BS06, a new field rock in Beishan, Gansu Province of China (Chen *et al*., 2012). The shape of the rock sample was cylindrical with a diameter of 50mm and a height of 100mm. As for the basic mechanical parameters of the rock sample, the density was 2.70g/cm^3, the uniaxial compressive strength was 160-170MPa, the average compressive strength was 161.47MPa, the average Poisson's ratio was 0.15 and the elastic modulus was 61.2GPa.

For this research, the flat-joint contact model was used to construct the mesoscopic analysis model of the granite, as shown in Figure 5. Prior to the calculation, the meso-mechanical parameters assumed by the model needed to be assigned. Through the numerical experiment, the macro mechanical parameters obtained by the calculation were compared with the lab test results. By constantly adjusting the meso-mechanical parameters, when the calculation and test results were basically the same, the meso-mechanical parameters obtained after debugging could be applied to the subsequent calculation and analysis of the model. After repeated debugging was matched, when the meso-mechanical parameters shown in Table 1 were used, the compressive strength, Young's modulus and Poisson's ratio were calculated to be 167.4MPa, 62.5GPa and 0.16, respectively, under the uniaxial compression conditions. These were in good agreement with the experimental results. Therefore, the micro-mechanical parameters of the model in Table 1 accurately describe the mechanical properties of the the test granite.

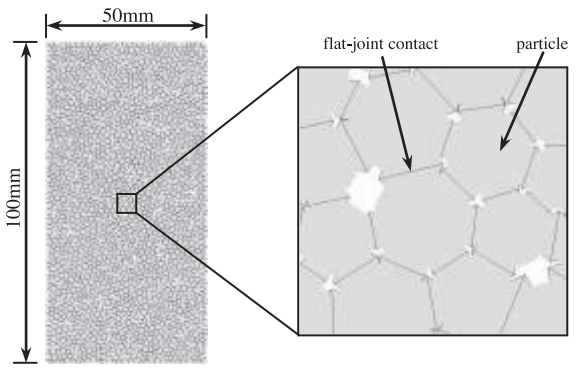

Fig. 5. Granite meso-analysis model

Table 1. Meso-mechanical parameters of calculation model

Particle					
Minimum particle radius R_{min}/mm	Particle radius ratio R_{rat}	Bulk density ϱ/(kg·m^{-3})	Friction coefficient μ	Young's modulus E_c/GPa	Stiffness ratio of normal and shear k_n/k_s
0.62	1.66	2700	0.50	80	1.25

Flat-joint contact model								
Number of discrete segments	Young's modulus $\bar{E}_c$/GPa	Stiffness ratio of normal and shear $\bar{k}_n/\bar{k}_s$	Friction coefficient $\bar{\mu}$	Bond tensile strength σ_b/MPa	Standard deviation of bond tensile strength / MPa	Bond cohesion c_b/MPa	Standard deviation of bond cohesion /MPa	Bond frictional angle ϕ_b/°
4	80	1.25	0.50	22	2.2	400	40	10.0

Focusing on the granite mesoscopic analysis model constructed above, the uniaxial tension, uniaxial compression and triaxial compression numerical experiments were carried out. Among them, the confining pressure (CP) of triaxial compression was set to 5 ~ 60MPa. Based on the principle of servo mechanism, the wall rate was constantly adjusted to maintain a continuous confining pressure. In order to ensure a quasi-static loading state, the loading rate should be set small enough. For this research, the loading rate of uniaxial tension $\dot{\varepsilon}$ was set to 0.164, while the loading rate of uniaxial compression and triaxial compression $\dot{\varepsilon}$ was set to 1.0. These loading rates for the simulation tests of uniaxial tension, uniaxial compression and triaxial compression, could achieve both quasi-static loading state and computational efficiency.

3.2 Fracture mechanism

Under the conditions of uniaxial tension, uniaxial compression and triaxial compression, the distribution of cracks in the meso-analysis model of the granite is shown in Figure 6. The red line represents the tensile crack, which was generated by the tensile failure of the flat-joint contact model; the blue line represents the shear crack generated by the shear failure of the flat-joint contact model. Figure 7 shows the macroscopic fracture distribution of granite samples after uniaxial tension and triaxial compression (CP=60MPa). With the combination of Figure 6 and Figure 7, the fracture mechanism of granite can be analyzed and understood.

Figure 6(a) shows that under the uniaxial tension condition, when the granite meso-analysis model is destroyed, the cracks are produced by the tension failure on the flat-joint contact model, which is perpendicular to the axial loading direction. The results show that the macroscopic fault zone perpendicular to the axial loading direction of the granite under uniaxial tension condition is mainly formed by the cohesive tension on the grain boundary, and the macroscopic fracture surface is rugged. In Figure 7(a), the failure of the granite specimen under the uniaxial tension condition shows that the failure of the sample is a full-section fracture, which is mainly roughed along the coarse-grained joint of the rock and mineral composition. Macroscopically, the macro fracture surface is perpendicular to the loading axis. Therefore, it can be concluded that the calculated results of granite meso-analysis model are consistent with the experimental results under tensile conditions.

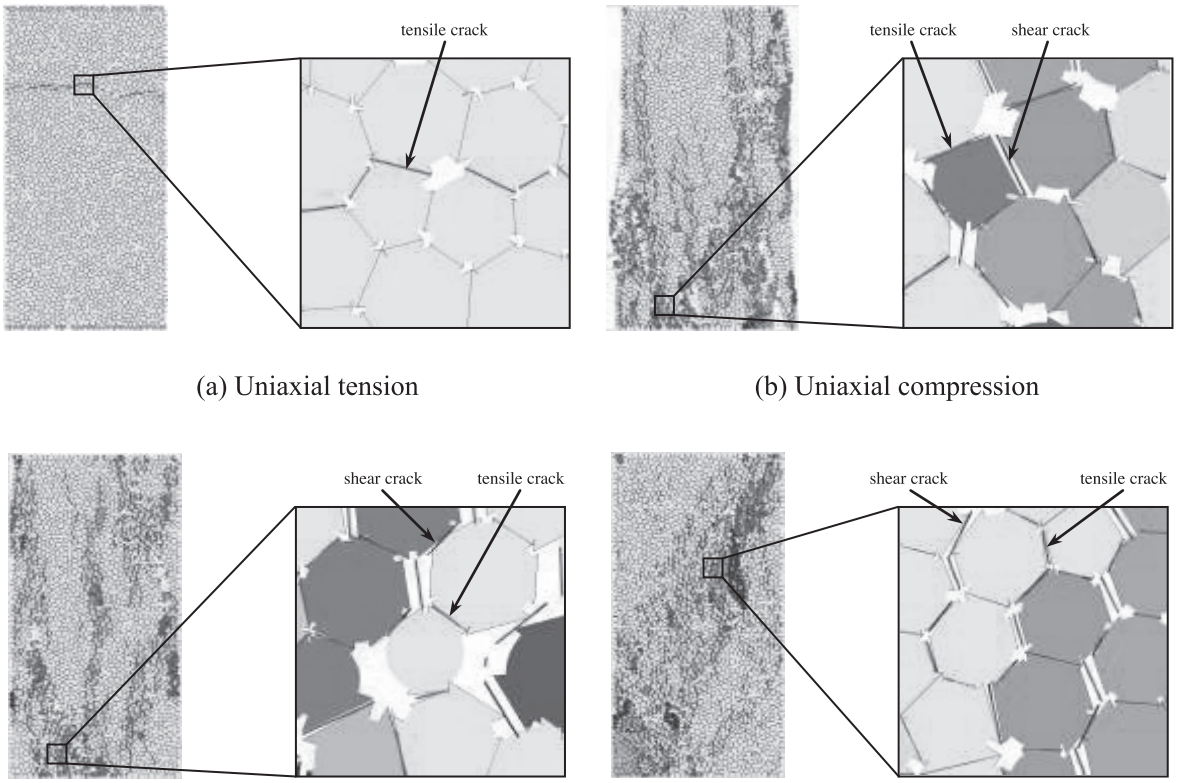

(a) Uniaxial tension (b) Uniaxial compression

(c) Triaxial compression (confining pressure 5 MPa) (d) Triaxial compression (confining pressure 60 MPa)

Fig. 6. Crack distribution of granite meso-analysis model

Figure 6(b) shows the distribution of cracks in a granite micro-analysis model under uniaxial compression loading failure. As shown, there are tensile and shear failures in the line segment of the flat-joint contact model, but the tensile failure is the main factor. When the specimen is destroyed, the penetration crack produced by the failure of the flat-joint contact model leads to a macroscopic splitting failure along the axial direction of the specimen.

Figure 6(c) shows the crack distribution of the granite meso-analysis model under low confining pressure (CP=5MPa). Similar to the uniaxial compressive loading failure, the failure mode of the model is the macroscopic splitting failure, and the penetration crack is produced by the failure of the flat-joint contact model under the low confining pressure loading. This eventually leads to the macroscopic fracture surface along the axial direction. However, unlike the uniaxial compression test, the shear failure rate increases with the increase of confining pressure, but the tensile crack is dominant.

Figure 6(d) shows the crack distribution of the granite meso-analysis model under high confining pressure (CP=60MPa). As shown, the failure of the line on the flat-joint contact model is still the coexistence of tensile failure and shear failure. However, with the further increase of confining pressure, the number and proportion of shear failure are further improved. The macroscopic fracture zone, with an angle to the loading axial direction, is formed from the top to the bottom of the specimen, which results in the macroscopic shear failure of the granite under high confining pressure. Figure 7(b) shows the triaxial compressive failure test results of granite samples under confining pressure of 60MPa. The results are in agreement with the calculated results. The macroscopic fracture surface mainly penetrates the top and bottom of the specimen and has a certain angle with the loading axis.

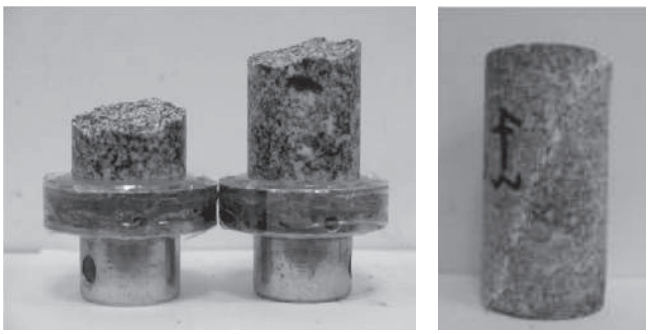

(a) Uniaxial tension (b) Triaxial compression

Fig. 7. Failure condition of specimen

A comparison of results shows that they are approximatively in agreement with each other, which indicates that it is feasible to study the mechanical characteristics of brittle rock by using the flat-joint contact model.

3.3 Strength characteristics

The calculated result of the meso-analysis model of granite under the conditions of uniaxial tension shows that when the tensile strain reaches 0.0163%, the model reaches peak tensile strength, which is about 9.07MPa. After the peak tensile strength, the stress decreases rapidly with the increase of the strain, and the calculation model shows strong brittle tensile failure characteristics.

Figures 8 and 9 show the stress-strain curves of the granite meso-analysis model under uniaxial compression and triaxial compression loading. As shown, with the increase of confining pressure, the peak compressive strength of the model increases and the strain value corresponding to the peak compressive strength also increases. Under the uniaxial compression condition, after the model reaches the peak strength, the stress-strain curve decreases rapidly, and the specimen shows strong brittle characteristics. At low confining pressure (ie CP=5MPa and 10MPa), the stress-strain curve gradually shows a strain-softening phenomenon, and the brittleness of the specimen is weakened. With the confining pressure continuously increasing (ie CP=50MPa 60MPa), the failure characteristics of the specimen changed from brittle failure to ductile failure.

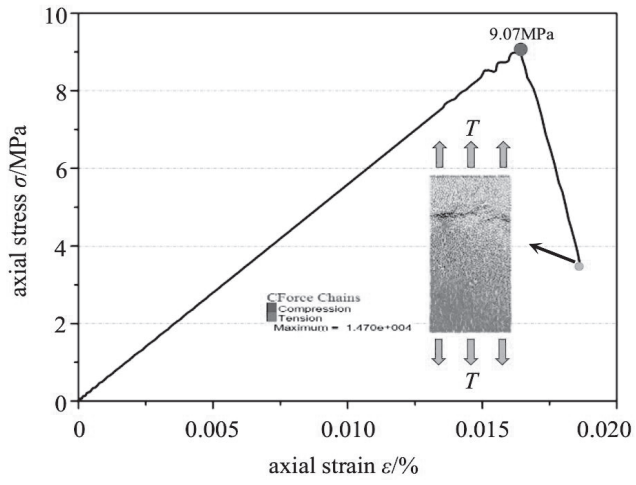

Fig. 8. Stress-strain curve of tensile test of granite meso-analysis model

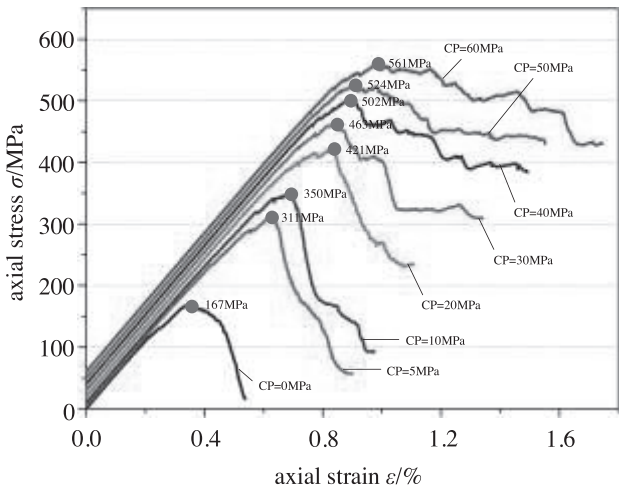

Fig. 9. Stress-strain curve of compression test of granite meso-analysis model

Based on a large number of uniaxial, triaxial test data and field test results, Hoek & Brown (1980) used the trial-and-error method to derive Hoek-Brown strength criterion by analyzing and modifying Griffith theory, revealing the relationship of the ultimate principal stress between rock block and rock mass. After constantly improving the amending, Hoek *et al.* (2002) developed it into the generalized Hoek-Brown strength criterion. According to uniaxial tension, uniaxial compression, triaxial compressive peak strength and corresponding confining pressure of granite meso-analysis model, the Hoek-Brown strength criterion is fit into σ_1-σ_3 Cartesian coordinate system. Finally, the Hoek-Brown strength fitting curve of granite meso-analysis model is obtained, as shown in Figure 10. The fitting function is shown as Equation (16):

$$\sigma_1 = \sigma_3 + 167\left(41.98\frac{\sigma_3}{167} + 2.09\right)^{0.395}, \qquad (16)$$

where σ_1 and σ_3 are the maximum and minimum principal stresses when a rock mass is destroyed, respectively, and the correlation coefficient of the fitting curve is 0.967. It can be seen from Figure 10 that the ratio of the uniaxial tensile to uniaxial compressive strength (σ_t/σ_{ucs}) of the model is about 0.054 (9.07MPa/167MPa), which shows that the model has strong brittle characteristics.

A series of uniaxial, uniaxial and triaxial compression test results for granite specimens are also given in Figure 10. It can be seen that the distribution of experimental data is similar to that of the Hoek-Brown strength criterion. The distribution range and calculation results are also similar. The experimental results (Chen *et al.,* 2012) show that the tensile strength of granite is 6.95~12.33MPa, the average tensile strength is 9.53MPa, the uniaxial compressive strength is 160~170MPa, and the average uniaxial compressive strength is 161.47MPa. Therefore, the ratio of uniaxial tensile to uniaxial compressive strength (σ_t/σ_{ucs}) equals 0.059. It ranges from 0.041 to 0.077. The ratio of uniaxial tensile to uniaxial compressive strength (σ_t/σ_{ucs}) of the granite meso-analysis model is 0.054, which is consistent with the experimental results. However, if the traditional particle model is used to match the macroscopic mechanical parameters under uniaxial compression, the ratio of uniaxial tensile to uniaxial compressive strength (σ_t/σ_{ucs}) is about 0.325 (53.0MPa/162.8 MPa), which is higher than the experimental result. Therefore, it is feasible to study the mechanical characteristics of brittle rock by using the flat-joint contact model based on the calculation results of the granite meso-analysis model.

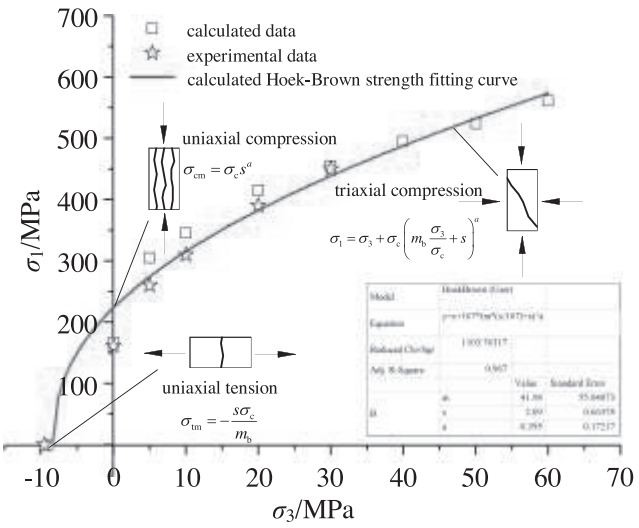

Fig. 10. Hoek-Brown strength fitting curve of granite meso-analysis model

4. Discussion

Based on the particle flow method, in addition to the flat-joint contact model presented in this paper, there is the clumped particle model (CPM) and grain-based model (GBM). They can be used to study the mechanical characteristics of brittle rock. As shown in Figure 11, the minimum diameter of the circular particle is 0.62mm, and the ratio of maximum to minimum radius of the particle is 1.66, which is consistent with the particle size parameter of the granite meso-analysis model in this study.

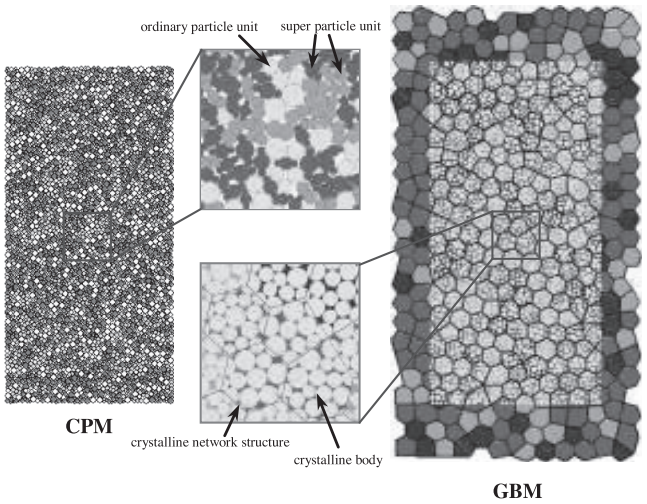

Fig. 11. Clumped particle model and equivalent crystal model

The principle of constructing the meso-analysis model of brittle rock by CPM is that the ordinary (circular or spherical) particle unit in the model is replaced by an irregular super-particle unit, which is composed of a plurality of relatively small ordinary particle units, thereby reproducing the self-locking effect between the rock particles. In this process, the volume of the ordinary particle unit and the super particle unit are equal before and after the replacement. Cho *et al.* (2007), Ding & Zhang (2014) studied the mechanical properties of various types of brittle rocks by CPM. However, there are still some defects in CPM. Cho *et al.* (2007) showed that the minimum ratio of uniaxial tensile to uniaxial compressive strength calculated by CPM is usually about 0.07, which is still a little higher (0.03 ~ 0.04) than that of the general hard brittle rock test results. In addition, the lower the σ_t/σ_{ucs} is, the more complex the irregular super-granule unit is constructed and the more the number of ordinary particle units is needed to construct a super-particle unit, which greatly reduces the overall calculation efficiency of the model.

The principle of constructing the meso-analysis model of brittle rock by GBM is such that the spatial geometrical information of the crystal network structure or the particle model - constructed by an ordinary particle unit - is divided into close-adjacent crystalline bodies by the crystalline network structure. Then, by changing the particle contact model into a smooth joint model, the GBM can be constructed. This can characterize the real microstructure of the rock. Zhou *et al.* (2015) verified the suitability and reliability of the GBM in the study of the characteristics of brittle rock mechanics. The research revealed the fracture mechanism and strength characteristics of a rock under loading condition from the mesoscopic viewpoint. GBM can also reproduce the self-locking effect between rock particles, and it is capable of obtaining a relatively low ratio of uniaxial tensile to uniaxial compressive strength (σ_t/σ_{ucs}). For example, the σ_t/σ_{ucs} obtained by the GBM calculation in Zhou *et al.* (2015) is 0.047. However, the irregular mineral grains in GBM are characterized by a crystalline body, which in turn is constructed from circular particles. In order to obtain more accurate calculation results, the crystalline body often needs circular particles of smaller size to build. In the simulation of rock samples containing fine particles (diameter<1mm), the number of circular particles needed for modeling will greatly increase, resulting in a significant decrease in overall computational efficiency of the model. Figure 11 shows that the average particle size of the crystal is 5.0mm, which is characteristic of coarse grains.

In this study, the contact interface is discretized into a segment with bond strength when the flat-joint contact model is used to build the granite meso-analysis model. With the gradual destruction of the bond strength, the interface state can be changed from a fully bonded state to a partially bonded, non-adhesive or friction state. When the bond is completely destroyed, the contact interface morphology still exists. It can resist the relative motion of particles in the process of rotation, thereby reproducing the self-locking effect (Figure 6). In the traditional particle model, the parallel bond model will be eliminated after being destroyed, so that the contact interface length is zero and no longer has the ability to resist the relative rotation during particle movement. Thus, it cannot produce a self-locking effect. In this paper, each particle is divided into a single irregular polygon by the flat-joint contact model, and the crystal structure of a mineral particle is characterized, which greatly improves the overall efficiency of the model.

In general, the mechanical behavior of brittle rock can be accurately reconstructed by using a GBM or flat-joint contact model, but the latter has certain advantages in terms of computational efficiency.

5. Conclusions

In this study, the flat-joint contact model was used to construct the granite meso-analysis model, which can reflect the structural characteristics of mineral particles. Combined with the test data of Beishan granite from Gansu Province, the suitability and reliability of the flat-

joint contact model in the study of the characteristics of brittle rock mechanics were verified by comparing the calculated results with those of the test results. The outcomes clearly show the fracture mechanism and strength characteristics of granite under a loading condition from a meso-mechanical viewpoint. The main conclusions are as follows:

(1) Under uniaxial tension condition, the macroscopic fracture surface, which is approximately perpendicular to the loading axial direction, is formed by the cohesive tension failure on the grain boundaries.

(2) Under conditions of uniaxial compression or low confining pressure triaxial compression, the macroscopic fracture surface parallel to the loading axial direction is mainly caused by the cohesive tension failure at the boundary of the mineral particles, leading to macroscopic splitting failure.

(3) Under a high confining pressure triaxial compression condition, the macroscopic fracture surface, which is at a certain angle with the loading axial direction, penetrates through the specimen. It is mainly composed of bond tension and shearing failure on the boundary of mineral grain, resulting in macroscopic shear failure of the rock.

(4) For hard and brittle rocks like granite, the calculation model based on the flat-joint contact model can reproduce a lower ratio of uniaxial tensile to uniaxial compressive strength, and its strength characteristics can be more reasonably described by using Hoek-Brown strength criterion.

ACKNOWLEDGEMENTS

This research was supported by the Fundamental Research Funds for the Central Universities (Grant No. FRF-TP-18-016A3) and the National Natural Science Foundation of China (Grant No. 51504016).

References

Chen, L., Liu, J., Wang, C., Wang, L., Wang, X. & Wang, J. (2012). Study of acoustic emission characteristics of Beishan deep granite under different stress conditions. Chinese Journal of Rock Mechanics and Engineering, **31**(supp. 2): 3618-3624.

Cho, N., Martin, C.D. & Sego, D.C. (2007). A clumped particle model for rock. International Journal of Rock Mechanics & Mining Sciences, **44**(7): 997-1010.

Cundall, P.A. & Strack, O.D.L. (1979). A discrete numerical model for granular assemblies. Geotechnique, **29**(1): 47-65.

Diederichs, M. (2000). Instability of hard rock masses: the role of tensile damage and relaxation. University of Waterloo.

Ding, X. & Zhang, L. (2014). A new contact model to improve the simulated ratio of unconfined compressive strength to tensile strength in bonded particle models. International Journal of Rock Mechanics and Mining Sciences, **69**(3): 111-119.

Go, G.H., Lee, S.R., Kim, Y.S. & Yoon, S. (2014). A new thermal conductivity estimation model for weathered granite soils in Korea. Geomechanics and Engineering, **6**(4): 359-376.

Hazzard, J.F. & Young, R.P. (2000). Simulating acoustic emissions in bonded-particle models of rock. International Journal of Rock Mechanics and Mining Sciences, **37**(5): 867-872.

Hoek, E. & Brown, E.T. (1997). Practical estimates of rock mass strength. International Journal of Rock Mechanics and Mining Sciences, **34**(8): 1165-1186.

Hoek, E. & Brown, E.T. (1980). Underground Excavations in Rock. Institution of Mining and Metallurgy, London, England.

Hoek, E., Carranza-Torres, C. & Corkum, B. (2002). Hoek-Brown failure criterion-2002 edition. Proceedings of the Fifth North American Rock Mechanics Symposium, Toronto, 267-273.

Kazerani, T. & Zhao, J. (2010). Micromechanical parameters in bonded particle method for modelling of brittle material failure. International Journal for Numerical and Analytical Methods in Geomechanics, **34**(18): 1877-1895.

Li, J., Zhou, Y., Sun, W., & Sun, Z. (2019). effect of the interaction between cavities and flaws on rock mechanical properties under uniaxial compression. Advances in Materials Science and Engineering, Volume 2019, Article ID 1242141, 9 pages.

Miao, S., Yang, Z., Long, C. & Tan, W. (2013). Equivalent plastic parameters optimization research on CWFS failure criterion model of brittle hard rock. Chinese Journal of Rock Mechanics and Engineering, **32**(supp. 1): 2600-2605.

Potyondy, D.O. & Cundall, P.A. (2004). A bonded-particle model for rock. International Journal of Rock Mechanics and Mining Sciences, **41**(8): 1329-1364.

Su, H. & Li, C.H. (2011). Mesoscopic numerical simulation of acoustic emission experiment in rock compression failure under different confining pressures. Journal of University of Science and Technology Beijing, **33**(11): 1312-1318.

Tang, C., Zhu, W. & Yang, T. (2014). Impact of rock microstructures on failure processes- Numerical study based on DIP technique. Geomechanics and Engineering, **7**(4): 375-401.

Wu, S. & Xu, X. (2016). A study of three intrinsic problems of the classic discrete element method using flat-joint model. Rock Mechanics and Rock Engineering, **49**(5): 1813-1830.

Zhou, H., Yang, Y., Xiao, H., Zhang, C. & Fu, Y. (2013). Research on loading rate effect of tensile strength property of hard brittle marble-test characteristics and mechanism. Chinese Journal of Rock Mechanics and Engineering, **32**(9): 1868-1875.

Zhou, J., Zhou, Y., & Gao, Y. (2018). effect mechanism of fractures on the mechanics characteristics of jointed rock mass under compression. Arab Journal of Science and Technology, 43: 3659-3671.

Zhou, L., Chu, X., Zhang, X. & Xu, Y. (2016). Numerical investigations on breakage behaviour of granular materials under triaxial stresses. Geomechanics and engineering, **11**(5): 639-655.

Zhou. Y., Gao, Y., Wu, S., Yan, Q. & Sun, H. (2015). An equivalent crystal model for mesoscopic behaviour of rock. Chinese Journal of Rock Mechanics and Engineering, **34**(3), 511-519.

Zhou, Y., Zhang, G., Wu, S., & Zhang, L. (2018). The effect of flaw on rock mechanical properties under the Brazilian test. Kuwait Journal of Science, **45**(2): 89-99.

Submitted : 03/02/2018
Revised : 27/03/2018
Accepted : 02/04/2018

نموذج اتصال مفصل مسطح وتحليل بيني للخصائص الميكانيكية للصخور الهشة

[1]يو تشو، [1]نينجبين تشن، [2]لي وانغ، [3]جيانوانغ لي، [1]تيانهوا وو

[1]المختبر الرئيسي لوزارة التعليم للتعدين الفعال وسلامة مناجم المعادن، جامعة العلوم والتكنولوجيا، بكين، الصين

[2]شركة باور شينا للجسور والطرق، محدودة، بكين، الصين

[3] شركة السكك الحديدية الصينية المكتب 16، بكين، الصين

المؤلف: *163.com@18692939718*

الملخص

في الوقت الحالي، يصعب محاكاة نموذج الجسيمات التقليدية للخصائص الميكانيكية للصخور الهشة مثل بنية الجسيمات ونسبة الشد أحادي المحور إلى قوة الضغط أحادية المحور (σ_t/σ_{ucs}). استناداً إلى نظرية تدفق الجسيمات ورمز تدفق الجسيمات (PFC)، يتم استخدام نموذج الأتصال المفصلي المسطح لبناء نموذج تحليل الجرانيت البيني، والذي يمكن أن يعكس ميزات الهيكل المعدني. تمت محاكاة أوضاع فشل الصخور تحت التوتر أحادي المحور والضغط أحادي المحور والضغط ثلاثي المحور ومقارنتها بالنتائج التجريبية. وأظهرت النتائج أن هذا النموذج ذو أداء جيد في دراسة ميكانيكا الصخور الهشة. وأظهر البحث كذلك، بالنسبة للصخور الهشة مثل الجرانيت، أنه يمكن إعادة إنتاج النسبة المنخفضة من الشد أحادي المحور إلى قوة الضغط أحادية المحور للصخور باستخدام نموذج الأتصال المفصلي المسطح لبناء نموذج حسابي، ويمكن وصف خصائص قوته باستخدام معيار قوة هوك براون.